Star formation suppression and bar ages in nearby barred galaxies

P. A. James⋆ and S. M. Percival

Astrophysics Research Institute, Liverpool John Moores University, IC2, Liverpool Science Park, 146 Brownlow Hill, Liverpool L3 5RF, UK

ABSTRACT

We present new spectroscopic data for 21 barred spiral galaxies, which we use to explore the effect of bars on disc star formation, and to place constraints on the characteristic lifetimes of bar episodes. The analysis centres on regions of heavily suppressed star formation activity, which we term 'star formation deserts'. Long-slit optical spectroscopy is used to determine $H\beta$ absorption strengths in these desert regions, and comparisons with theoretical stellar population models are used to determine the time since the last significant star formation activity, and hence the ages of the bars. We find typical ages of ∼1 Gyr, but with a broad range, much larger than would be expected from measurement errors alone, extending from ∼0.25 to >4 Gyr. Low-level residual star formation, or mixing of stars from outside the 'desert' regions, could result in a doubling of these age estimates. The relatively young ages of the underlying populations coupled with the strong limits on the current star formation rule out a gradual exponential decline in activity, and hence support our assumption of an abrupt truncation event.

Key words: Galaxies: spiral – galaxies: stellar content – galaxies: structure.

1 INTRODUCTION

Bars are a common feature in disc galaxies, with ∼30 per cent of galaxies having strong bars that are clearly apparent in their optical morphologies (Knapen, Shlosman & Peletier 2000; Marinova & Jogee 2007; Nair & Abraham 2010), ∼50 per cent of galaxies in the Sloan Digital Sky Survey (SDSS) showing bars (Barazza, Jogee & Marinova 2008; Aguerri, Méndez-Abreu & Corsini 2009), and at least 60 per cent showing evidence of stellar bars in near-infrared (near-IR) imaging (Seigar & James 1998; Grosbøl, Patsis & Pompei 2004; Menéndez-Delmestre et al. 2007). There has been extensive discussion of the possible central role of bars in the so-called 'secular evolution' of disc galaxies (Kormendy & Kennicutt 2004), with the main debate centring on the possibility that bars build central bulge components at the expense of disc material (Pfenniger & Norman 1990; Friedli & Benz 1993; Cheung et al. 2013). In this picture, bars are a major factor in constructing the morphological sequence of changing bulge-to-disc ratio first pointed out by Hubble (1926). Recently, an additional aspect of this debate has emerged, with the suggestion that bars can play a controlling aspect in the overall star formation (SF) rate of disc galaxies, and may indeed be a significant player in the transformation of galaxies between the 'blue cloud' and the 'red sequence' populations first identified by Strateva et al. (2001) and Baldry et al. (2004). The possibility that bars may decrease total SF rates within a galaxy was proposed by Tubbs (1982) and has seen renewed interest recently in the proposal

of Haywood et al. (2016) that a turn-down in the SF rate of the Milky Way may have been driven by the simultaneous formation of the Galactic bar. This suggestion has also received confirmation in the context of cosmological studies of large samples of galaxies at low and intermediate redshifts; Gavazzi et al. (2015) and Consolandi (2017) find that that the SF rate versus stellar mass relation of strongly barred galaxies is offset significantly towards lower SF values, compared to unbarred galaxies. Similarly, Kim et al. (2017) use a large sample of galaxies from the SDSS to demonstrate that the strongly barred galaxies show significantly lower SF activity than their unbarred counterparts.

Our work in this area started with the analysis of the spatial distributions of SF in the discs of barred and unbarred galaxies using narrow-band $H\alpha$ imaging from the $H\alpha$GS survey (James et al. 2004). In James, Bretherton & Knapen (2009), this imaging was used to demonstrate that strongly barred galaxies, particularly of earlier Hubble types, exhibit a radial pattern of SF that is radically different to that of their unbarred counterparts. The defining feature within the barred galaxies is the almost complete suppression of SF in the radial range 'swept out' by the bar, which we term the 'star formation desert' (SFD). This is accompanied in many cases by an *increase* in SF both at the centre of the bar and in a ring just outside the ends of the bar, with the bar-end increase generally being larger than that found in nuclei, in terms of emission line flux and inferred SF activity.

Strong supporting evidence for this SFD phenomenon was provided from a completely independent line of analysis by Hakobyan et al. (2016). They analysed the radial distributions of ∼500 core-collapse supernovae in nearby disc galaxies, which showed clear

⋆ E-mail: P.A.James@ljmu.ac.uk

Table 1. Galaxy properties and observing details. See Section 2 for descriptions of column entries.

Name	Classification	Velocity (km s^{-1})	Distance (Mpc)	Bar PA (°)	Slit PA (°)	$T_{int,tot}$ (s)	SFD image
UGC 3685	SB(rs)b	1797	28.3	131	0	10 800	Hα
NGC 2487	SB(r)c	4827	66.8	45	315	10 800	SDSS
NGC 2523	SB(r)bc	3471	51.5	125	60	8400	SDSS
NGC 2543	SB(s)b	2470	35.9	90	180	7200	Hα
NGC 2595	SAB(rs)c	4324	59.9	158	260	7200	Hα
NGC 2712	SB(r)b	1815	28.1	28	350	6000	Hα
NGC 3185	(R)SB(r)a	1238	20.0	113	320	7200	Hα
NGC 3346	SB(rs)cd	1250	20.4	95	0	13 200	SDSS
NGC 3367	SB(rs)c	2944	42.1	72	170	7200	Hα
NGC 3485	SB(r)b	1436	24.0	40	130	7200	SDSS
NGC 3507	SB(s)b	979	13.8	120	30	13 200	SDSS
NGC 3729	SB(r)a	1060	19.4	20	290	6000	SDSS
NGC 3811	SB(r)cd	3105	46.4	30	267	6000	Hα
NGC 4123	SB(r)c	1286	25.3	105	15	7200	SDSS
NGC 4779	SB(rs)bc	2855	41.9	5	280	7200	SDSS
NGC 4999	SB(r)b	5634	78.7	60	330	6000	SDSS
NGC 5350	SB(r)b	2311	36.5	130	20	6000	SDSS
NGC 5375	SB(r)ab	2373	37.0	170	260	6000	SDSS
NGC 5698	SBb	3629	54.1	168	70	6000	Hα
NGC 5806	SAB(s)b	1347	22.4	172	30	8400	Hα
NGC 5970	SB(r)c	1957	30.9	80	350	7200	SDSS

suppression of SN numbers in the radial ranges swept out by strong bars, just as predicted by the SFD hypothesis. Interestingly, this suppression effect was only found in Sa to Sbc barred galaxies, and not those of type Sc and later, consistent with our findings from Hα profiles in James et al. (2009), and equivalent findings of 'bar bimodality' by Nair & Abraham (2010) and Hakobyan et al. (2014) (see also the theoretical predictions of Villa-Vargas, Shlosman & Heller 2010), with late-type bars being associated with concentrated SF along the length of bars, rather than deserts. Further confirmation came from the recent study of Abdurro'uf & Akiyama (2017), who found lower specific SF rates in the central regions, but not in the outer regions, for the barred galaxies within a sample of 93 low-redshift massive spiral galaxies.

A possible mechanism for the SF suppression effect of bars was identified by Reynaud & Downes (1998). In a detailed study of the nearby strongly barred SBb galaxy NGC 1530, they found that the bar induces strong shocks and shearing gas motions, which they conclude should be sufficiently strong to stabilize the gas against collapse and subsequent SF. Similarly, Verley et al. (2007) concluded that gas velocities induced by bars may be sufficient to stabilize even high gas densities against SF in the immediate vicinity of the bar. An alternative possibility is suggested by the study of Spinoso et al. (2017). They simulate the evolution of a Milky Way-like spiral galaxy, of estimated type Sb or Sc, and find that the formation of a bar efficiently depletes gas in a region of radius ~2 kpc, corresponding to the maximum radial length of the bar. Deciding between these possibilities of stabilization or complete removal of gas from SFD regions is beyond the scope of this paper, but is an interesting question for future study.

1.1 Stellar populations in star formation desert regions

In James & Percival (2016), we presented our first detailed study of stellar populations within SFD-hosting galaxies, using long-slit optical spectroscopy of four strongly barred early-type galaxies,

NGC 2543, NGC 2712, NGC 3185, and NGC 3351. This study confirmed the complete suppression of SF within the SFD region in these four galaxies; while some low-level diffuse line emission was detected, this showed line ratios and a smooth spatial distribution that can be much more naturally explained by an old stellar population, for example, post-asymptotic giant branch stars (James & Percival 2015); see also Stasińska et al. (2008), Sarzi et al. (2010), Yan & Blanton (2012) and Bremer et al. (2013). After correcting for this weak line emission, we fitted the remaining absorption-line spectra by a model that assumed an initially constant SF rate, followed by a sharp truncation in SF activity; the one free parameter in the model was the epoch at which this truncation occurred. The most important conclusion of this analysis was that SF was suppressed long ago in the SFD regions of these four galaxies, and that this epoch differs significantly between the four, with a range of ~1 – >4 Gyr.

This paper builds on the work presented by James & Percival (2016) by substantially increasing the sample size of observed galaxies. New long-slit spectroscopic data are presented and analysed for a total of 21 barred galaxies, comprising repeated observations for 3 of the galaxies from James & Percival (2016) and new observations for 18 previously unstudied systems.

2 OBSERVATIONS

The properties of the 21 barred galaxies in the present study are listed in Table 1, including classification and distance properties which were taken from the NASA/IPAC Extragalactic Database (NED). Column 1 of Table 1 contains the galaxy name; column 2 the galaxy classification; column 3 the heliocentric recession velocity; column 4 the adopted galaxy distance, based on a Hubble constant of 73 km s^{-1} Mpc^{-1} and a correction for infall velocities generated by the Virgo cluster; and column 5 the adopted bar position angle. Column 6 gives the position angle of the slit in the new spectroscopic observations presented in this paper and column 7

the total integration time in seconds for these observations. Finally, column 8 gives the source of the imaging observations used for initial classification and for the measurement of bar parameters. An entry of 'H α' in this column means that our own H α imaging, from James et al. (2004), was used to identify the galaxy as possessing a SFD, and to measure the radial extent of the SFD region when extracting integrated spectra. *R*-band images from the same source were used to determine the bar position angle. An entry of 'SDSS' in column 8 means that SDSS York et al. (2000) *gri* colour images (Lupton et al. 2004) were used for all these tasks.

In comparison with our previous work (James & Percival 2016), we are now able to present not only a much larger sample, but also higher quality and more uniform spectroscopic data, with our earlier observations having been seriously affected by poor observing conditions. Galaxies in the new sample lie at somewhat greater distances (range 14–80 kpc, cf. 10–40 kpc for the earlier study), and cover a wider range of Hubble type. In James & Percival (2016), one galaxy was of type Sa and the other three Sb, and all were strongly barred with SB classifications. In this study, we present results for two Sa, one Sab, nine Sb, two Sbc, five Sc and two Scd galaxies. Of these 21 galaxies, 18 have strongly barred SB classifications, and the other 3 are considered intermediate-strength SAB types. We checked whether any galaxies within this sample are known to host a double bar (otherwise known as a 'bar-within-a-bar') by cross-checking with the latest version of the list maintained by Peter Erwin, first published as Erwin (2004). Possibly surprisingly, only NGC 5806 is a known double-bar host, which may indicate that the SFD phenomenon is less common or less marked in galaxies with these central components.

The new observations presented here are long-slit optical spectra, taken with the intermediate dispersion spectrograph (IDS) on the 2.5-metre Isaac Newton Telescope (INT) at the Observatorio del Roque de Los Muchachos on La Palma in the Canary Islands. The observing time was allocated to proposal I/2016/P1 by the UK Panel for the Allocation of Telescope Time. The observing dates allocated to the project were the seven nights of 2016 March 3–9 inclusive, with usable data being taken on all nights. Occasional thin cirrus cloud affected three nights, and the first two nights suffered from haze due to Saharan dust in the atmosphere above the observatory; however, photometric conditions were not required for these observations.

The observing set-up of the IDS was as follows. The grating used was R900V, which has a blaze wavelength of 5100 Å. The EEV10 blue-sensitive CCD detector was used to maximize sensitivity in the region of H β absorption, the most important feature for the present investigation. The slit width for all galaxy observations was 1.5 arcsec, corresponding to 2.9 pixels or 1.8 Å in the spectral direction, given a dispersion of 0.63 Å pixel^{-1}. The spatial resolution for this setup is 0.4 arcsec pixel^{-1}, and an unbinned CCD readout was used. The unvignetted wavelength coverage was 1518 Å about a central wavelength of 4900 Å. The slit was generally aligned to be perpendicular or close to perpendicular to the bar of each galaxy (see Table 1) and so, in general, observations were not made at the parallactic angle. However, all of the important parameters for the present analysis are derived from line equivalent width (EW) values, which are unaffected by atmospheric dispersion effects.

Spectrophotometric standard star observations, using sources selected from the observatory standards list[1] were made two to three times per night through a wide slit (4–5 arcsec) to provide flux

calibration. However, this calibration was not required for any of the results presented here.

3 DATA REDUCTION

3.1 Basic reduction and spectral extraction

Data reduction of our long-slit spectroscopy was performed using STARLINK software (Currie et al. 2014). All stages, i.e. bias subtraction, flat fielding, correction of spectra for minor rotation and spatial distortion effects, sky background subtraction, wavelength calibration using a copper neon + copper argon arc lamp, and flux calibration from spectrophotometric standard observations were completely standard will not be described further here. More details are given in James & Percival (2016). H α narrow-band imaging, where available (see Table 1), was used to define the apparently emission-line free region from which the 'desert' spectra were extracted. In other cases, SDSS *gri* colour images were used for this purpose. In all cases, two desert regions were extracted for each galaxy, one on either side of the nucleus, and the radial ranges were conservatively restricted to ensure that all emission from the nuclear regions was excluded.

The new analysis presented here resulted in 42 spectra, one from each side of the nucleus of each of the 21 galaxies. As noted above, this sample includes three of the four galaxies discussed in James & Percival (2016), but we have obtained new, deeper spectroscopy for these galaxies, and the updated measurements are used here.

The spectral analysis methods used were described in full in James & Percival (2016). The main parameters extracted from the spectra were absorption line EW values. The most important feature, due to its strong age sensitivity, is H β 4861 Å, but in order to take account of age-metallicity degeneracy in the strength of this feature, we also measured the predominantly metallicity sensitive Mgb feature centred on 5176 Å. EW values for these features were determined by direct integration on the reduced and extracted spectra, using the wavelength ranges for features and continuum defined by Trager et al. (1998).

Rotational velocities and stellar velocity dispersion could, in principle, have an effect on measured line indices. For the present sample, galaxy rotation will not have a large effect; the galaxies observed are generally close to face-on, and the spectra are extracted separately from opposite sides of the nucleus so the rotational difference between these regions is not an issue. Departure from flat rotation curves in the extracted regions, and velocity dispersion, will lead to moderate broadening of absorption features, but this will at most be at the 100 km s^{-1} level. We conservatively tested the effects of this by convolving BaSTI solar-abundance models with Gaussian functions with a σ of 150 km s^{-1}, and found a completely negligible impact on the indices used here, which is understandable given that the indices used are EWs summed over broad bandpasses (29 Å for the most important index, H β, while 150 km s^{-1} is equivalent to only 2.4 Å at the wavelength of H β).

There is one case of a galaxy that was observed in 2016 March observing run, but where no results are presented in this paper. This was the galaxy NGC 2604, of type SB(rs)cd. In this case, strong emission lines with ratios consistent with expectations for SF regions (Baldwin, Phillips & Terlevich 1981) were observed at all locations along the slit, so there is nothing that can be termed a SFD in this galaxy, and these lines are sufficiently strong to prevent the accurate measurement of absorption line indices, both at H α and H β. This is not entirely surprising; NGC 2604 is described as an 'interacting galaxy with deformed arms' by Miyauchi-Isobe &

Figure 1. SDSS *gri* images of four of the observed barred galaxies, showing the range of Hubble type classifications of the full sample. Top left-hand panel: NGC 3185, classification (R)SB(r)a. Top right-hand panel: NGC 4999, classification SB(r)b. Bottom left-hand panel: NGC 4123, classification SB(r)c, for which the Hβ absorption strength could be extracted only for one side of the SFD. Bottom right-hand panel: NGC 2604, classification SB(rs)cd, which shows strong SF at all locations, including within the bar and in the regions swept out by the bar, and hence is not included in the main analysis, as explained in Section 3.1.

Maehara (1998) in their study of ultraviolet excess galaxies, and the NED classification notes Wolf–Rayet and starburst characteristics. This galaxy also stands out as unusually blue in the SDSS *gri* colour composite image (see Fig. 1, lower right-hand panel); the blue colours extend over the whole of the galaxy, including the bar, so this is clearly an example where a bar has not suppressed SF anywhere in the disc or bar regions.

3.2 Correction for line emission

In James & Percival (2015), we used long-slit spectroscopy in the red part of the optical spectrum around the Hα emission line to show that almost all SFD regions in the 15 spiral galaxies studied exhibit low-level diffuse line emission. However, the Hα/[N II] line ratios are characteristic of LINER-type regions (Heckman 1980a; Baldwin et al. 1981), which conclusively excludes SF as the powering source behind this emission. We have extended that analysis to encompass a much larger sample of galaxies, including all 21 of the barred galaxies that are the subject of this paper. The analysis of the emission-line properties of the enlarged sample will be presented in a separate paper (James & Percival, in preparation). Here, it need only be noted that 9 of the present sample (those with an entry of 'Hα' in column 8 of Table 1) have emission line fluxes already published in James & Percival (2015), while the remaining 12 have emission-line properties that will be discussed in the future paper. There is no significant difference in the data quality or analysis methods between the two sub-samples.

As with James & Percival (2016), the emission-line measurements are essential for the accurate correction of emission-line

contamination of the Hβ absorption features. Without such correction, the Hβ strengths would be biased to significantly lower values, resulting in significant over-estimates of stellar population ages. To avoid this, we used the same iterative emission line correction procedure as in James & Percival (2016), which is based on the assumption of Case B line ratios for Balmer emission lines (Brocklehurst 1971; Hummer & Storey 1987). The second constraining assumption of the correction method is that the relative strengths of the Hα and Hβ absorption features should be consistent with the predictions of theoretical stellar population models (Pietrinferni et al. 2004; Percival et al. 2009). In the implementation of this correction, the Hβ absorption EW was measured first; this was then used to predict an Hα absorption EW based on the stellar population model; this absorption strength was used to give a corrected Hα emission line flux, and hence an Hβ line flux following the Case B assumption. The latter value was used to correct the initially measured Hβ absorption line EW, which was then taken as the starting point for the second iterative loop. In practice, the values converged quickly to values that satisfied the requirements of fitting the population models and expectations of the Case B assumption, after three or four iterations.

The results of the data reduction processes are shown in Table 2. Here, the first column gives the galaxy name, and the second column gives an identifier for the region from which the integrated SFD spectrum was taken. Column 3 gives the radial range in arcseconds of the region used to extract the spectrum, and column 4 the direction of offset of this region from the galaxy nucleus. Column 5 gives the initial measurement of the Hβ absorption-line EW in Å, with the associated error in column 6, and column 7 the Hβ EW after the iterative emission-line correction described in the previous paragraph.

Three of the SFD regions listed in Table 2 do not have values for the emission-line corrected Hβ EW. These regions lie in NGC 2487, NGC 2595, and NGC 4123, all of which have Hubble types of SBc (actually SABc for NGC 2595), and hence three of the latest types represented in the present sample. Thus, it is not surprising that these should have some residual SF in their central disc regions. One of these galaxies, NGC 4123, is shown in Fig. 1 (lower left-hand panel), which confirms that is indeed a transitional case between the 'true' SFD galaxies with red central discs shown in the upper row, and the starburst galaxy NGC 2604 to its right-hand side. The residual SF in the SFD regions of NGC 2487, NGC 2595, and NGC 4123 then explains the strong Hβ emission that prevents the measurement of the absorption feature in one half of the disc. The other half of the extracted SFD region in these three cases does give an acceptable iterative solution, generally resulting in a strong underlying absorption, indicating recent truncation ages and/or contamination by a younger stellar component.

The importance of accurate emission-line correction can be seen by comparing columns 5 and 7 of Table 2, with the Hβ EW values increasing following this correction by several times the measurement error in most cases. Indeed, about one-third of the regions would have unphysically small Hβ EW values without this correction, i.e. lower than could be fitted by any stellar population younger than the age of the Universe. The importance of this correction is not apparent from inspection of the spectra; the only ones that show any evidence for an emission peak at Hβ are those extracted from NGC 2595 and NGC 4123 with negative EW values in column 5 of Table 2. Otherwise, the emission is lost in the core of the absorption line profile.

Table 2. Observed regions and derived spectroscopic properties.

Galaxy	Region	Radial range (arcsec)	Direction	Hβ_{obs} (Å)	error	Hβ_{corr} (Å)
UGC 3685	SFD1	7.48–17.60	N	0.877	0.237	1.650
UGC 3685	SFD2	7.48–17.60	S	1.255	0.234	2.378
NGC 2487	SFD1	6.16–19.36	SE	1.558	0.248	2.481
NGC 2487	SFD2	6.60–14.08	NW	0.285	0.311	–
NGC 2523	SFD1	6.20–26.40	SW	1.559	0.199	1.985
NGC 2523	SFD2	6.20–21.60	NE	2.425	0.206	2.968
NGC 2543	SFD1	7.48–24.20	N	2.646	0.269	3.900
NGC 2543	SFD2	6.60–19.80	S	2.500	0.243	3.858
NGC 2595	SFD1	9.68–19.36	E	−0.276	0.568	–
NGC 2595	SFD2	13.20–26.40	W	2.335	0.491	3.861
NGC 2712	SFD1	6.16–21.56	S	1.776	0.207	2.747
NGC 2712	SFD2	7.48–20.68	N	1.323	0.233	2.529
NGC 3185	SFD1	9.68–21.56	SE	1.575	0.227	2.206
NGC 3185	SFD2	11.44–29.04	NW	1.257	0.211	1.877
NGC 3346	SFD1	6.60–10.56	N	1.050	0.361	2.552
NGC 3346	SFD2	5.28–11.44	S	0.630	0.289	2.068
NGC 3367	SFD1	5.28–9.68	N	0.905	0.298	2.239
NGC 3367	SFD2	5.72–10.12	S	0.605	0.287	2.005
NGC 3485	SFD1	5.28–14.52	NW	1.288	0.312	1.675
NGC 3485	SFD2	5.28–12.76	SE	2.759	0.257	3.353
NGC 3507	SFD1	6.16–23.76	NE	1.932	0.111	2.887
NGC 3507	SFD2	6.16–26.40	SW	1.997	0.105	2.894
NGC 3729	SFD1	4.40–14.10	NW	0.458	0.272	2.671
NGC 3729	SFD2	6.20–14,50	SE	0.873	0.250	2.919
NGC 3811	SFD1	5.28–10.56	W	1.915	0.302	2.901
NGC 3811	SFD2	5.28–10.56	E	2.036	0.308	2.657
NGC 4123	SFD1	8.80–26.40	N	0.811	0.287	3.204
NGC 4123	SFD2	8.80–23.32	S	−1.345	0.374	–
NGC 4779	SFD1	5.28–13.64	E	1.000	0.276	3.030
NGC 4779	SFD2	5.28–18.04	W	1.141	0.243	2.584
NGC 4999	SFD1	6.16–16.30	NW	1.777	0.289	2.865
NGC 4999	SFD2	6.16–20.68	SE	2.266	0.267	3.519
NGC 5350	SFD1	6.16–13.64	N	1.825	0.227	2.634
NGC 5350	SFD2	6.60–16.72	S	2.141	0.220	2.643
NGC 5375	SFD1	4.40–19.36	W	2.086	0.197	2.875
NGC 5375	SFD2	4.40–20.24	E	2.625	0.188	3.198
NGC 5698	SFD1	6.16–22.00	SW	1.540	0.294	2.347
NGC 5698	SFD2	7.04–19.36	NE	2.229	0.453	2.723
NGC 5806	SFD1	6.60–13.20	SW	1.989	0.152	2.805
NGC 5806	SFD2	6.60–11.44	NE	1.640	0.206	2.467
NGC 5970	SFD1	4.40–8.80	N	2.295	0.172	3.178
NGC 5970	SFD2	4.40–9.68	S	2.605	0.164	3.709

4 RESULTS

4.1 Star formation truncation ages from Hβ absorption strengths

Fig. 2 shows the main results from this paper. Each plotted point corresponds to the measured Hβ absorption EW value from an individual SFD region, after correction for line emission, plotted against the metallicity-sensitive Mgb EW values, derived from direct integration on the observed SFD spectra using the wavelength ranges specified by Trager et al. (1998). Error bars are derived from the photometric errors on this direct integration process, plus an additional error added in quadrature for the Hβ index only, to account for the additional uncertainty due to the emission-line correction. The points are overlaid on a grid derived from the BaSTI stellar population synthesis models (Pietrinferni et al. 2004; Percival et al. 2009). As in James & Percival (2016), these theoretical grids are derived from a model where SF began 13 Gyr ago, and
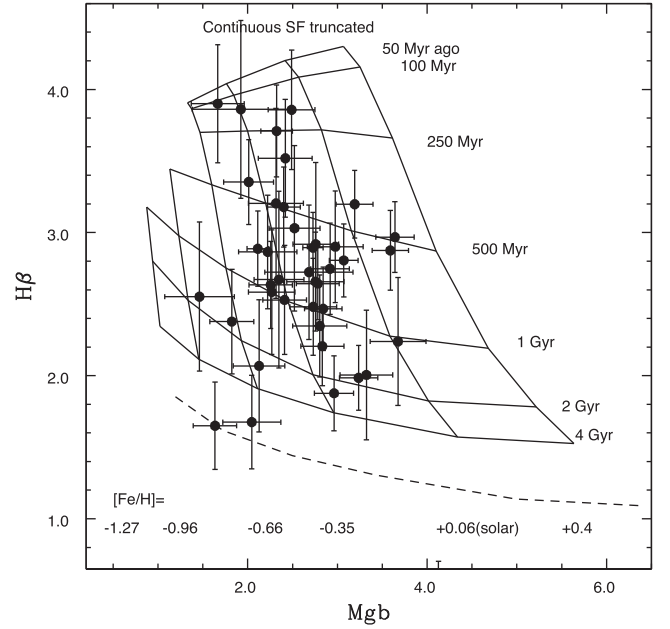

Figure 2. Observed emission-corrected Hβ and Mgb absorption strengths for the 39 SFD regions with well-measured Hβ EW values (see Table 2), overlaid on a grid of model predictions for different scaled solar metallicities and elapsed times since cessation of SF. The grid is derived from models with a spectral resolution of 1.0 Å, while the observations have a resolution of 1.83 Å. The observed range of SF truncation ages is from 0.1 to at least 4 Gyr, much larger than the expected range from uncertainties in age determinations. Even given this broad range of ages there is some indication of preferred time-scale, with points clustering around an age of ~1 Gyr.

proceeded at a constant rate until an abrupt and complete cessation of SF at a later epoch, which we allow us to vary from 4 Gyr ago (i.e. after 9 Gyr of steady SF) to only 50 Myr ago. The calculation of these models for a range of scaled solar metallicities from [Fe/H] of −1.27 to +0.4 (strongly sub-solar to significantly above solar) results in the grid points plotted in Fig. 2. The dashed line at the bottom of that figure is the locus of values for varying metallicity but a single population age of 14 Gyr, and effectively represents the physical limit for how weak the Hβ feature can become.

The main conclusions to draw from Fig. 2 are the following. Almost all of the points lie on the model grid, and all have physically plausible values of Hβ EW, i.e. they lie above the dashed line. The inferred truncation ages, i.e. the time since the last strong episode of SF cover virtually the full range of modelled values, with two regions lying above the oldest modelled age of 4 Gyr (although consistent with this value given the measurement error bars), while the most recently truncated region lies on the 100 Myr line. The spread in ages appears real, i.e. much greater than would be expected from measurement errors alone.

Fig. 3 shows the same information as Fig. 2, i.e. Hβ and Mgb line indices overlaid on the BaSTI model grid, but presented on a galaxy-by-galaxy basis. In this figure, index locations for pairs of regions that lie within the same galaxy are joined by dashed lines, with open circles representing the mean location in the index–index plane of each such pair. Eighteen galaxies had well-measured spectroscopic properties in SFD regions on both sides of the galaxy nucleus, and dashed lines are shown for all of these in Fig. 3. For the three galaxies previously mentioned, only one SFD spectrum could be reliably fitted to give absorption index determinations; in Fig. 3 these are plotted as circles with no associated dashed line.
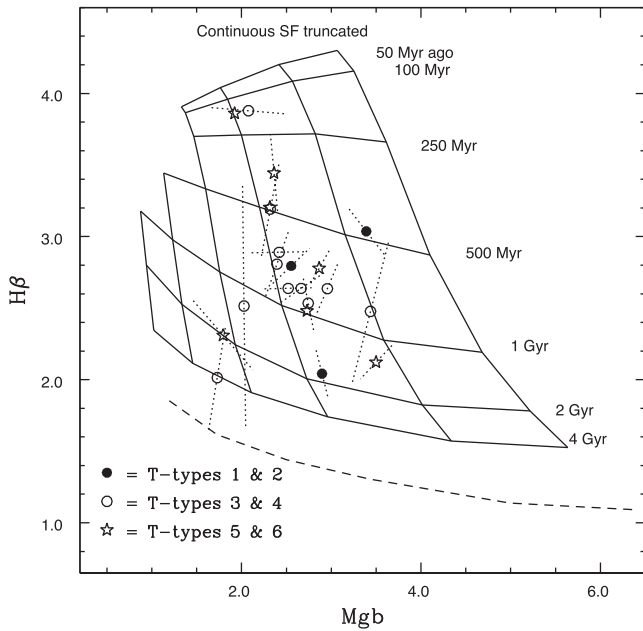
Figure 3. As Fig. 2, but now observations from SFD regions within the same galaxy are joined by dashed lines, with an open circle indicating the mean value of the derived age- and metallicity-sensitive parameters for that galaxy. Circles with no associated lines correspond to galaxies with only one measured SFD region. Different point types indicate the T-type classifications of the galaxies.

The data plotted in Fig. 3 enable us to test whether there are differences in stellar population properties for spatially separated parts of the SFD regions *within* a given galaxy. The generally short dashed lines in this figure indicate that any such inhomogeneities must be small, but we were able to quantify this impression by analysing the differences in observed corrected Hβ absorption strengths in the 18 galaxies. The median difference in EW was 0.334 Å, while the median error on the EW measurements for the same 18 galaxies (36 regions) was 0.336 Å. Thus, the differences seen within galaxies can be completely explained by the effects of measurement errors, and there is no evidence for any inhomogeneities in spectroscopic properties within the SFD regions of these 18 galaxies.

4.2 Analysis of SFD truncation ages as a function of galaxy type

In Fig. 3, galaxy classifications are indicated by different point types. There are no striking trends, but some inferences can still be drawn. Most of the main peak of galaxies within this plot, at inferred bar ages of 0.5–1 Gyr, are of type SBb, the classification that we have found to be most strongly associated with the SFD phenomenon. There is a slight excess of late-type galaxies with young bar ages, and/or larger fractional contamination of the investigated disc regions by young stars. Two of the three youngest, and three of the five youngest, have classifications of Sc or Scd. In addition, it should be remembered that there are three regions in Sc galaxies for which no absorption measurement was possible due to strong emission lines, and another late-type, NGC 2604, shows strong SF in all locations. So there is some trend for older populations, and earlier truncation epochs, in early-type galaxies. However, the main conclusion is that a broad range of truncation epochs, and hence inferred bar ages, is seen for all galaxy types. NGC 5806, the one galaxy identified as possessing a double bar, has entirely typical

properties for a galaxy of its type, with a truncation age of just under 1 Gyr.

4.3 Effects of residual star formation or stellar mixing

As an alternative to the models corresponding to complete truncation of SF at a given epoch, we also explored the effect of a downward step in SF, after which SF continued but only at 10 per cent of its previous rate. This was motivated by the findings of the Milky Way SF rate study of Haywood et al. (2016), who found just such a 90 per cent reduction in the SF rate, which they ascribe to the development of the strong Galactic bar. This obviously results in a larger fraction of young stars being present than for the earlier, complete truncation model, and so the epoch of such a step has to be pushed to earlier times to give an overall population that fits a given strength of Hβ absorption. To a fair approximation, we found that these 'step ages' are about twice the 'truncation ages' represented in the grid shown in Figs. 2–3, at least for the ages relevant to the bulk of the galaxy regions investigated here. Thus, complete truncation at 0.5 Gyr resembles a 90 per cent step at 1 Gyr, 1 Gyr matches 2 Gyr, and 2 Gyr matches 4 Gyr. Given the uncertainty of the appropriate step size to assume, we do not present full grids for this case, but the general results are instructive.

Note that many of our SFD regions show reductions in SF rate that are much more extreme than this 90 per cent value, as indicated by the weakness of any detected emission lines and the fact that any emission lines that are detected do not have ratios characteristic of SF. However, even if SF were to be completely suppressed within the SFD regions, as seems plausible, it is possible that young stars from elsewhere in the galaxy will be mixed in to the SFD region, for example, through bar-driven tidal torques. This would have the effect of introducing a younger stellar population without requiring ongoing SF within the region itself, and our 90 per cent step model is also useful to indicate the likely effects of such mixing on inferred bar ages.

4.4 Exponentially declining star formation histories

In Fig. 4, the SFD points from Fig. 3 are overplotted on a BaSTI model grid for an assumed exponentially declining SF history. For each grid point, SF is assumed to start 13.5 Gyr ago, and the different models are distinguished by exponential time constant τ and metallicity. Because of the lack of young, low-metallicity models in BaSTI, these models are now restricted to just four metallicity bins. The SFD stellar populations cluster around models with exponential decay times of ~ 6 Gyr, which has significant implications for the main analysis presented here. If the SFD regions really had SF histories with these exponential properties, the SF rate would be predicted still to be of the order of 10 per cent of the initial value, as the galaxy ages are only about two exponential decay times. Current SF at this rate is clearly ruled out by the weak emission lines seen as the defining feature of the SFD regions. Thus, the combination of relatively strong Hβ absorptions and stringent constraints on emission line fluxes requires there to have been a specific SF truncation event in these regions.

4.5 Simple stellar population models

Fig. 5 shows the data points from the previous two plots on a grid representing simple (single-age, single metallicity) stellar populations (SSPs), again from the BaSTI simulations. The galaxy spectra
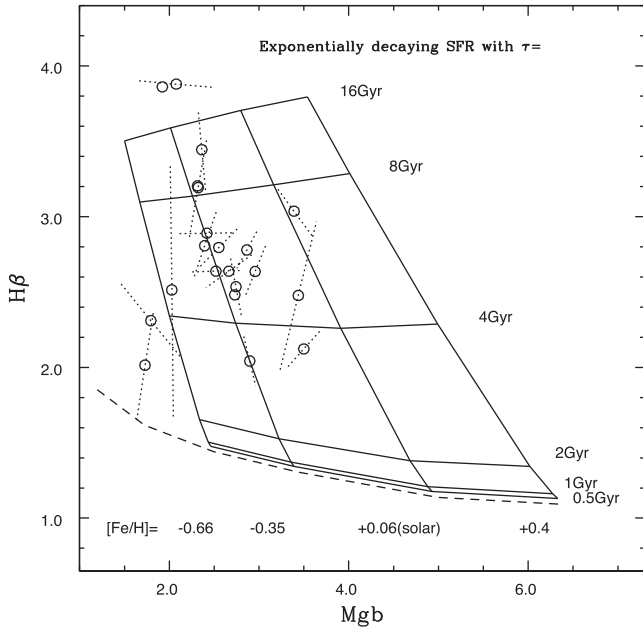
Figure 4. The line index points from Fig. 3 are here overlaid on a grid of index values for models with exponentially declining SF rates, starting 13.5 Gyr ago, with time constants indicated to the right-hand side of the grid.
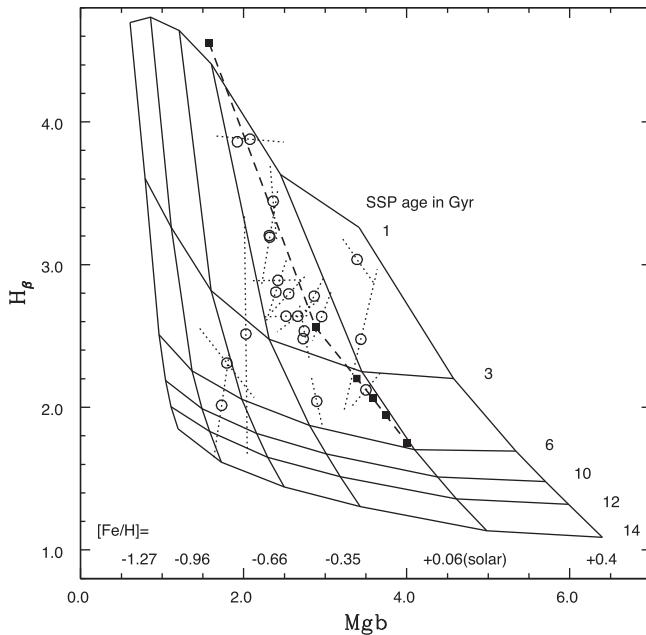

Figure 5. The line index points from Figs. 3 and 4 are overlaid on a grid of SSP models from BaSTI, with solar abundance points from MILES SSPs added as solid squares.

are best fitted by SSPs with ages between 1 and 8 Gyr, with most being about 2–3 Gyr.

It is important to test the robustness of the derived parameters, and particularly the separation of emission and absorption components, to our specific choice of population synthesis models for predicting absorption line features, given the well-known differences in the predictions of Balmer line absorptions between different spectral synthesis libraries. To investigate this, we did completely indepen-

dent spectral fits using the MILES empirical spectral library of Vazdekis et al. (2010). This showed that the separation of spectral lines into emission and absorption components was largely unaffected by the choice of model used; however, the derived ages of the corresponding populations do change significantly depending on which model is used, with BaSTI predicting younger ages than MILES. This systematic difference is the main uncertainty related to the choice of spectral model. We choose to continue to rely on BaSTI for our main age estimates, but since this is an important systematic, we have illustrated the differences in inferred BaSTI versus MILES ages in Fig. 5, Here, the filled squares show MILES predictions of H β and Mgb absorption strengths for SSPs with solar metallicity. This shows, for example, that the MILES 14 Gyr SSP corresponds to a BaSTI 6 Gyr model, though at the younger ages where the bulk of the SFD regions lie, the differences are much less marked, both in absolute and fractional terms. The most important conclusion from this comparison for the current work is that the separation of emission and absorption components is not significantly affected by the choice of stellar population model.

5 DISCUSSION

5.1 Comparison with theoretical predictions

The ages we find can be compared to the theoretical predictions from simulations. Some studies have concluded that bars overall tend to form in the early stages of galaxy evolution, and are subsequently stable and long-lived (Debattista et al. 2006; Curir, Mazzei & Murante 2008). However, Bournaud, Combes & Semelin (2005) find that gas-rich galaxies have bars that are short-lived, and they predict bar durations of 1–2 Gyr in Sb–Sc type galaxies. Athanassoula, Machado & Rodionov (2013) use *N*-body simulations to investigate the formation of bars within discs, and find long timescales of several Gyr for stable bars to become established, a conclusion that is supported by Martinez-Valpuesta et al. (2017). A key finding of Athanassoula et al. (2013) is that this time-scale is longer for discs with higher gas-mass fractions(see also Villa-Vargas et al. 2010), corresponding to later type classifications. This is in agreement with the weak trend we find in Fig. 3, discussed in Section 4.3, where the latest type galaxies have the most recently established SFD regions, or indeed still have SF throughout their bars and inner discs as seen for NGC 2604.

In their study of a simulated Milky Way-like spiral galaxy, Spinoso et al. (2017) found the bar started to form at $z = 0.4$, corresponding to a look-back time of 4.3 Gyr (Wright 2006), probably triggered by a minor merger; the bar stabilized and reached a maximum length at a look-back time of 1.3 Gyr ($z = 0.1$), at which time it had substantially depleted the gas reservoir in a central region of diameter 4 kpc. This depleted region persisted in their simulation to the present day, and strongly resembles our observed SFD regions in size and age.

5.2 Comparison with other observational estimates of bar ages

Many observational methods have been proposed in the literature to constrain bar ages and the evolution of bar properties with cosmological epoch. Jogee et al. (2004) studied the bar properties of a sample of high-redshift disc galaxies, finding that bars were in place early, and appeared to have long lifetimes, exceeding 2 Gyr. Other studies have inferred bar ages from detailed study of nearby barred galaxies. For example, Gadotti & de Souza (2005) measured the vertical velocity dispersion of the stellar component of strong

bars, finding high dispersions ($\sim$100 km s^{-1}) that developed only in simulated galaxy bars after several Gyr. In a subsequent paper (Gadotti & de Souza 2006), they used broad-band optical – near-IR colours to infer similarly old ages for the stellar populations that dominate bars. In both of these studies, the age ranges are rather larger than the SF truncation ages found for most of the galaxies in the present sample, although at least for the study of Gadotti & de Souza (2006), it should be noted that constraints quoted are for the stellar components of the bar, which could be very different to the age of the bar itself. Sánchez-Blázquez et al. (2011) studied two early type low-redshift barred galaxies, NGC 1558 (type SAB0) and NGC 1433 (SBab), concluding again that these bars are old and formed early in the lifetimes of their host galaxies. In a recent study, Font et al. (2017) analyse a large sample of barred galaxies with corotation radii derived from emission-line gas kinematics and find anomalous parameter correlations that they explain by invoking bar evolution over several Gyr, following a theoretical picture of gradual bar growth based on the models of Martinez-Valpuesta et al. (2017).

5.3 A possible time sequence of bar-induced activity

While there is still much work to be done on the details of the processes linked with bar activity in disc galaxies, it is possible to sketch out a possible time sequence of events following the first emergence of a bar, at least in terms of SF activity (see also Martinet & Friedli 1997). The most probable initial response is enhancement of SF activity, as indicated by several studies, following the early work of Heckman (1980b); see also Hawarden et al. (1986), Huang et al. (1996), Martinet & Friedli (1997), Aguerri (1999), Ellison et al. (2011), and Oh, Oh & Yi (2012). This short phase is likely to be marked by rapid transfer of gas to nuclear regions triggering strong nuclear SF, and SF along the bar itself, as is seen at the current epoch to be common in late-type (SBc–SBm) barred galaxies (see e.g. NGC 2604 in Fig. 1).

After this, the bar strengthens, lengthens, and suppresses SF over large radial range; this is the SFD phenomenon discussed in this paper. This is a long-lived phase compared with the initial enhancement of SF, with Gyr time-scales indicated by this analysis and the prevalence of this SF pattern in early and intermediate Hubble type barred galaxies. During this phase, SF continues in the nucleus, and is induced in a ring around the bar ends, but these do not compensate for the complete suppression within the large area of the SFD, and so the overall effect is a reduction in the integrated SF rate of galaxy (James et al. 2009).

While this SFD phase is long-lived, the lack of ages >4 Gyr in this study imply that the SFD phase does not last indefinitely. This raises the question of what happens after SFD phase: Can the galaxy return to having a full SF disc, and potentially undergo multiple barred phases, or does the SF suppression propagate outwards to encompass the bar-end ring and outer disc, resulting in a red-sequence passive spiral or lenticular galaxy? We plan to address this possibility in our future work.

6 CONCLUSIONS

The main conclusions of this study are as follows:

(i) We confirm the SFD phenomenon, i.e. the strong suppression of SF in disc regions swept-out by strong galaxy bars using deep spectroscopy for a sample of 22 galaxies.

(ii) We are able to determine H β absorption line EW values for disc regions of all but one of the observed galaxies.

(iii) Absorption line strengths can be fitted by stellar populations with a constant SF rate prior to an abrupt and complete cessation of SF, with the epoch of this truncation event as the one free parameter in the models.

(iv) The truncation epoch varies significantly between different galaxies, over a range extending from 0.1 to more than 4 Gyr, and some evidence for a preferred age of about 1 Gyr.

(v) Truncation ages derived from independent regions within the same galaxy are mutually consistent, given the expected measurement errors.

(vi) Stellar populations appear homogeneous within the SFD regions; we find no evidence for differences in spectroscopic properties on opposite sides of the nucleus within individual galaxies of this sample.

(vii) If the SF suppression is only 90 per cent effective, or if there is an equivalent level of radial mixing of young stars from outside the SFD region, the truncation epoch is shifted earlier, by a factor of approximately 2 in age.

(viii) Gradually declining exponential SF histories fail to reconcile the population ages with the lack of current SF, supporting models with a specific epoch where SF is strongly truncated.

(ix) There is some indication of later and/or less complete truncation of SF in later-type barred galaxies, consistent with theoretical modelling of galaxies with higher gas-mass fractions, for example, Athanassoula et al. (2013).

Overall, these conclusions confirm and are fully consistent with those derived for a pilot study of four galaxies in James & Percival (2016).

More work is needed to address several aspects of the processes discussed here. One remaining question concerns the physical process underlying the SFD phenomenon: Is gas present in these regions, but stabilized against collapse, for example, by bar-induced turbulence, or has it been removed completely through bar-driven torques? Detailed mapping of gas densities within galaxy discs exhibiting the SFD phenomenon is required to answer this question.

A second uncertainty concerns the continued development of the SFD galaxies. Are there cases where the SF suppression continues to propagate outwards through the rings and outer discs, resulting in completely passive disc galaxies, without the involvement of external environmental or active galactic nucleus-driven processes? What would the final galaxy state be as a result of such secular processes, and, for example, would the bars and rings seen in the SFD systems survive to the passive stage? These are complex questions, requiring further theoretical input, but on the observational side, Integral Field Unit surveys yielding two-dimensional stellar population maps of large samples of galaxies seem likely to play a strong role.

REFERENCES

Abdurro'uf, Akiyama M., 2017, MNRAS, 469, 2806

Aguerri J. A. L., 1999, A&A, 351, 43

Aguerri J. A. L., Méndez-Abreu J., Corsini E. M., 2009, A&A, 495, 491

Athanassoula E., Machado R. E. G., Rodionov S. A., 2013, MNRAS, 429, 1949

Baldry I. K., Glazebrook K., Brinkmann J., Ivezić Ž., Lupton R. H., Nichol R. C., Szalay A. S., 2004, ApJ, 600, 681

Baldwin J. A., Phillips M. M., Terlevich R., 1981, PASP, 93, 5

Barazza F. D., Jogee S., Marinova I., 2008, ApJ, 675, 1194

Bournaud F., Combes F., Semelin B., 2005, MNRAS, 364, L18

Bremer M., Scharwächter J., Eckart A., Valencia-S. M., Zuther J., Combes F., Garcia-Burillo S., Fischer S., 2013, A&A, 558, A34

Brocklehurst M., 1971, MNRAS, 153, 471

Cheung E. et al., 2013, ApJ, 779, 162

Consolandi G., 2017, PhD Thesis

Curir A., Mazzei P., Murante G., 2008, A&A, 481, 651

Currie M. J., Berry D. S., Jenness T., Gibb A. G., Bell G. S., Draper P. W., 2014, Astron. Data Anal. Softw. Syst. XXIII, 485, 391

Debattista V. P., Mayer L., Carollo C. M., Moore B., Wadsley J., Quinn T., 2006, ApJ, 645, 209

Ellison S. L., Nair P., Patton D. R., Scudder J. M., Mendel J. T., Simard L., 2011, MNRAS, 416, 2182

Erwin P., 2004, A&A, 415, 941

Font J. et al., 2017, ApJ, 835, 279

Friedli D., Benz W., 1993, A&A, 268, 65

Gadotti D. A., de Souza R. E., 2005, ApJS, 629, 797

Gadotti D. A., de Souza R. E., 2006, ApJS, 163, 270

Gavazzi G. et al., 2015, A&A, 580, A116

Grosbøl P., Patsis P. A., Pompei E., 2004, A&A, 423, 849

Hakobyan A. A. et al., 2014, MNRAS, 444, 2428

Hakobyan A. A. et al., 2016, MNRAS, 456, 2848

Hawarden T. G., Mountain C. M., Leggett S. K., Puxley P. J., 1986, MNRAS, 221, 41P

Haywood M., Lehnert M. D., Di Matteo P., Snaith O., Schultheis M., Katz D., Gómez A., 2016, A&A, 589, A66

Heckman T. M., 1980a, A&A, 87, 152

Heckman T. M., 1980b, A&A, 88, 365

Huang J. H., Gu Q. S., Su H. J., Hawarden T. G., Liao X. H., Wu G. X., 1996, A&A, 313, 13

Hubble E. P., 1926, ApJ, 64, 321

Hummer D. G., Storey P. J., 1987, MNRAS, 224, 801

James P. A., Percival S. M., 2015, MNRAS, 450, 3503

James P. A., Percival S. M., 2016, MNRAS, 457, 917

James P. A. et al., 2004, A&A, 414, 23

James P. A., Bretherton C. F., Knapen J. H., 2009, A&A, 501, 207

Jogee S. et al., 2004, ApJ, 615, L105

Kim E., Hwang H. S., Chung H., Lee G.-H., Park C. C S. B., Kim S. S., 2017, ApJ, 845, 93

Knapen J. H., Shlosman I., Peletier R., 2000, ApJ, 529, 93

Kormendy J., Kennicutt R. C., 2004, ARA&A, 42, 603

Lupton R., Blanton M. R., Fekete G., Hogg D. W., O'Mullane W., Szalay A., Wherry N., 2004, PASP, 116, 133

Marinova I., Jogee S., 2007, ApJ, 659, 1176

Martinet L., Friedli D., 1997, A&A, 323, 363

Martinez-Valpuesta I., Aguerri J. A. L., González-García A. C., Dalla Vecchia C., Stringer M., 2017, MNRAS, 464, 1502

Menéndez-Delmestre K., Sheth K., Schinnerer E., Jarrett T. H., Scoville N. Z., 2007, ApJ, 657, 790

Miyauchi-Isobe N., Maehara H., 1998, Publ. Natl. Astron. Obs. Japan, 5, 75

Nair P. B., Abraham R. G., 2010, ApJ, 714, L260

Oh S., Oh K., Yi S. K., 2012, ApJS, 198, 4

Percival S. M., Salaris M., Cassisi S., Pietrinferni A., 2009, ApJ, 690, 427

Pfenniger D., Norman C., 1990, ApJ, 363, 391

Pietrinferni A., Cassisi S., Salaris M., Castelli F., 2004, ApJ, 612, 168

Reynaud D., Downes D., 1998, A&A, 337, 671

Sánchez-Blázquez P., Ocvirk P., Gibson B. K., Pérez I., Peletier R. F., 2011, MNRAS, 415, 709

Sarzi M. et al., 2010, MNRAS, 402, 2187

Seigar M. S., James P. A., 1998, MNRAS, 299, 672

Spinoso D., Bonoli S., Dotti M., Mayer L., Madau P., Bellovary J., 2017, MNRAS, 465, 3729

Stasińska G. et al., 2008, MNRAS, 391, L29

Strateva I. et al., 2001, AJ, 122, 1861

Trager S. C., Worthey G., Faber S. M., Burstein D., González J. J., 1998, ApJS, 116, 1

Tubbs A. D., 1982, ApJ, 255, 458

Vazdekis A., Sánchez-Blázquez P., Falcón-Barroso J., Cenarro A. J., Beasley M. A., Cardiel N., Gorgas J., Peletier R. F., 2010, MNRAS, 404, 1639

Verley S., Combes F., Verdes-Montenegro L., Bergond G., Leon S., 2007, A&A, 474, 43

Villa-Vargas J., Shlosman I., Heller C., 2010, ApJ, 719, 1470

Wright E. L., 2006, PASP, 118, 1711

Yan R., Blanton M. R., 2012, ApJ, 747, 61

York D. G. et al., 2000, AJ, 120, 1579

This paper has been typeset from a TEX/LATEX file prepared by the author.